Journal of Magnetic Resonance 341 (2022) 107263

Contents lists available at ScienceDirect

Journal of Magnetic Resonance

journal homepage: www.elsevier.com/locate/jmr

Current limitations of solid-state NMR in carbohydrate and cell wall research

Wancheng Zhao [a], Fabien Deligey [a], S. Chandra Shekar [a], Frederic Mentink-Vigier [b], Tuo Wang [a,*]

[a] Department of Chemistry, Louisiana State University, Baton Rouge, LA 70803, USA
[b] National High Magnetic Field Laboratory, Tallahassee, FL 32310, USA

ARTICLE INFO

Article history:
Received 14 April 2022
Revised 18 June 2022
Accepted 28 June 2022
Available online 2 July 2022

Keywords:
Solid-state NMR
Dynamic nuclear polarization
DNP
Carbohydrate
Cell wall
Polysaccharide

ABSTRACT

High-resolution investigation of cell wall materials has emerged as an important application of biomolecular solid-state NMR (ssNMR). Multidimensional correlation experiments have become a standard method for obtaining sufficient spectral resolution to determine the polymorphic structure of carbohydrates and address biochemical questions regarding the supramolecular organization of cell walls. Using plant cellulose and matrix polysaccharides as examples, we will review how the multifaceted complexity of polysaccharide structure is impeding the resonance assignment process and assess the available biochemical and spectroscopic approaches that could circumvent this barrier. We will emphasize the ineffectiveness of the current methods in reconciling the ever-growing dataset and deriving structural information. We will evaluate the protocols for achieving efficient and homogeneous hyperpolarization across the cell wall material using magic-angle spinning dynamic nuclear polarization (MAS-DNP). Critical questions regarding the line-broadening effects of cell wall molecules at cryogenic temperature and by paramagnetic biradicals will be considered. Finally, the MAS-DNP method will be placed into a broader context with other structural characterization techniques, such as cryo-electron microscopy, to advance ssNMR research in carbohydrate and cell wall biomaterials.

© 2022 Elsevier Inc. All rights reserved.

1. Introduction

Carbohydrates and glycoconjugates regulate cellular recognition and communication, serve as energy sources, and provide structural support to the cells of many organisms [1]. These biologically important functions are often driven by the structural characteristics of carbohydrate polymers, such as glycosidic linkages and conformations. However, complex carbohydrates are difficult to characterize in their native physical state and have remained under-investigated, unlike proteins and nucleic acids. Solid-state NMR (ssNMR) has a long history (approximately 50 years) of being employed to characterize cellulose-based materials, such as fibers, derivatives, and lignocellulosic biomass [2–4]. Early studies typically relied on the extensive use of 1D ^{13}C spectra to resolve different allomorphs, quantify their contents, and determine the crystallinity of cellulosic materials. Another important application, as summarized in a recent review [5], is to understand the supramolecular organization of cell walls and biofilms in many organisms across biological kingdoms. In these studies, multidimensional (2D and 3D) correlation approaches are often required to achieve sufficient resolution for investigating cellular samples [5–8]. Because ssNMR can address questions of polymer structure and packing on the angstrom-to-nanometer length scale, the results complement the information provided by many diffraction and imaging methods that focus on the nanoscale and mesoscale.

The high-resolution studies of cell wall materials were built on a toolbox that combines ssNMR methods commonly used in both structural biology and polymer research [9]. Unlike for purified biomolecules, the complexity and heterogeneity of native biomaterials prevent the construction of atomistic models or of an ensemble of interchanging structures [10]. As shown by multiple studies of fungal and plant cell walls [11–13], only the model-based physical and structural principles that regulate the assembly and function of biomolecules can be obtained, similar to the outcomes expected for polymer ssNMR. However, the ever-growing dataset is evolving striking resemblance to that used in NMR structural biology. For example, a recent study has compared the lignin-carbohydrate packing interfaces in grasses, hardwoods, and softwoods, proposing structural models based on more than a thousand site-specific data of polymer interactions and dynamics [11].

The goal of this review is to highlight the underexplored directions where method development is urgently needed. We will critically review the intrinsic structural complexity underlying the

* Corresponding author.
E-mail address: tuowang@lsu.edu (T. Wang).

https://doi.org/10.1016/j.jmr.2022.107263
1090-7807/© 2022 Elsevier Inc. All rights reserved.

difficulty in analyzing carbohydrate polymers and recognize the immediate need for calculation methods for converting underused structural constraints into atomistic models. We will then selectively address questions regarding the applications of magic-angle spinning dynamic nuclear polarization (MAS-DNP) in cell wall research. Sections are also devoted to discussing the potential opportunities opening up for each of the current limitations.

2. Overview of experimental approach

Typically, uniformly $^{13}C/^{15}N$-labeled cell wall materials or whole cells are measured using 2D and 3D correlation experiments to examine biopolymer structure and cell wall assembly (Fig. 1) [5]. The most useful experiments for resonance assignment are *J*- or dipolar-based refocused INADEQUATE experiments, which unambiguously display the carbon connectivity in each type of sugar units. Cellular carbohydrates usually come with structural polymorphism to a high extent; a phenomenon that can be closely traced via peak multiplicity in 2D/3D $^{13}C–^{13}C/^{15}N$ spectra. From the peak intensities, which are represented as the peak volumes or areas, the composition of the cell wall molecules can be quantified. It is always beneficial to cross-compare these values with other analytical methods such as chromatography and mass spectrometry (MS). To examine the sub-nanometer physical packing, ssNMR offers a large collection of long-range correlation experiments, including but not limited to PDSD, CORD, CHHC, and PAR [14–16]. Molecular dynamics are examined using relaxation, dipolar couplings, and exchange NMR, depending on the timescale of the dynamics of interest. Spectral-editing techniques are effective for selecting molecules with unique structural motifs (for example, aromatics and nitrogen sites), rigidity or mobility, and water association, against the bulk of the cell wall [17–19].

Depending on the growth condition, plants can be grown in solution media containing ^{13}C-glucose or chambers containing $^{13}CO_2$ [20]. The former is usually limited to young seedlings grown in dark to avoid isotope dilution by ^{12}C, while the latter has a broader range of applications regarding the plant species and developmental stages. Well-established protocols are also available for labeling other organisms such as fungi, bacteria, and algae. Sample handling should be carefully designed to minimize structural perturbation, notably by avoiding chemical treatment and harsh physical processing techniques such as ball-milling. Typically, a razor blade is used to cut the tissues into millimetric pieces to allow for an even distribution of weight in the rotor during magic-angle spinning (MAS). The native hydration status is another crucial consideration in biomolecular ssNMR. Because the hydroxyl groups of carbohydrates efficiently associate with water molecules, it is not surprising that highly similar spectral features were found in both never-dried cell walls and in samples submitted a dehydration-rehydration cycle. This has been observed in the primary cell walls of *Arabidopsis*, the secondary cell walls of spruce and eucalyptus, and microalgae named *Parachlorella* [11,21,22]. However, moderate irreversible alternations induced by dehydration have been detected in sorghum and pine. The changes mainly happen to the hemicellulose (xylan and mannan) located on the packing interface with other polymers (lignin and cellulose) [23,24]. Native and fresh cells or tissues are recommended whenever available.

3. Resonance assignment impeded by structural complexity

Like protein structural determination by ssNMR, analysis of a ^{13}C-labeled cell wall sample begins with resonance assignment, which also turned out to be the most challenging step. The cell wall is typically the most rigid component and can be selected against intracellular molecules using experimental schemes based on cross-polarization (CP). However, the spectrum is still overcrowded due to the coexistence of a large variety of carbohydrates in the cell wall. The structural polymorphism of carbohydrate polymer further leads to peak multiplicity. Over the past decade, we have progressively uncovered the link between the structural and spectroscopic characteristics, which are summarized in Fig. 2 and detailed below.

First, non-cellulosic polysaccharides have highly diverse patterns of covalent linkages. When a linkage occurs to a carbon site, its ^{13}C isotropic chemical shift becomes larger by several ppm (also called downfield shift). In solids, this principle was demonstrated by systematically tracking the signals of matrix polysaccharides in the model grass *Brachypodium distachyon* [26]. Fig. 2a shows an example of arabinose, which is a monosaccharide unit com-

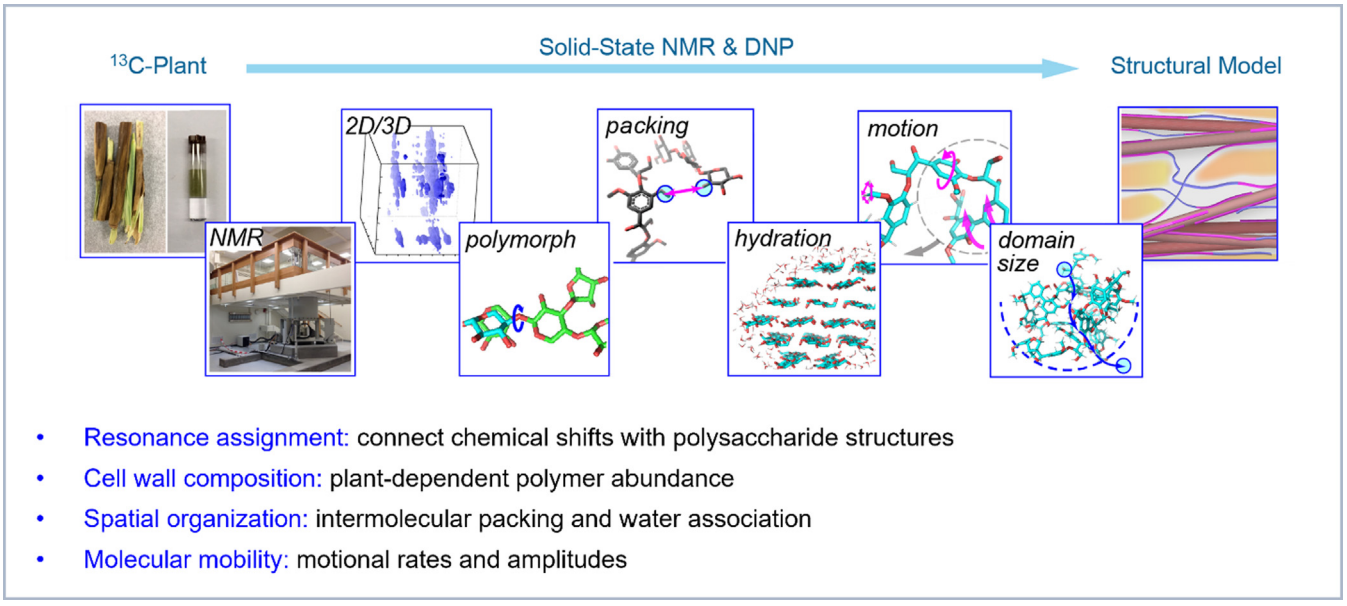

Fig. 1. Schematic representation of ssNMR studies of cell wall materials. Plants are taken as an example, and only cell wall polysaccharides and lignin are shown here for illustration. Some panels of the figure are adapted from reference [25].

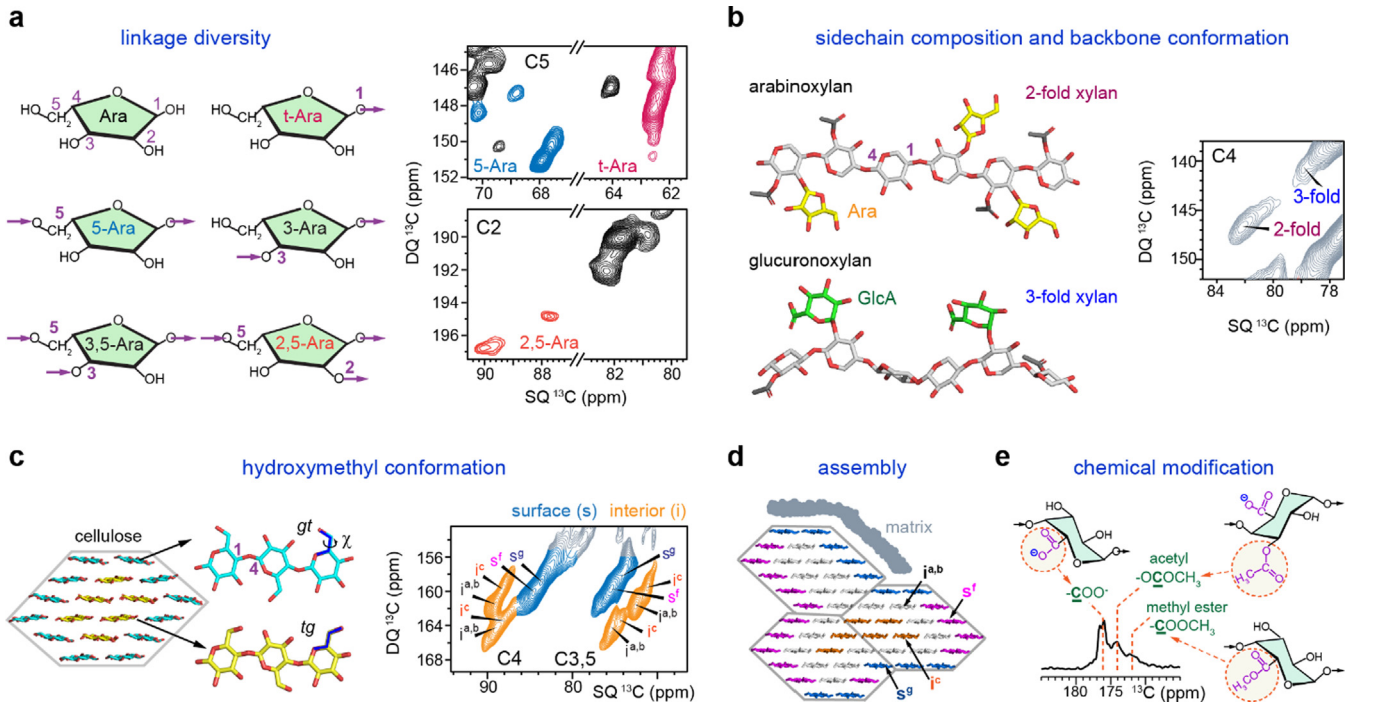

Fig. 2. Structural complexity and peak multiplicity of plant carbohydrates. (a) Linkage diversity demonstrated on the arabinose (Ara) unit. The C5 and C2 regions of Ara are shown using a 2D refocused J-INADEQUATE spectrum measured on *Brachypodium*. The key linkage sites are labeled in the structure, with the corresponding NMR signals color-coded in the spectra. (b) Simplified examples of arabinoxylan and glucuronoxylan containing arabinose and glucuronic acid (GlcA) sidechains. Note that the two-fold and three-fold helical screw symmetries of the xylan backbone have been observed for both arabinoxylan and glucuronoxylan. The C4 region of xyloses differentiates signals from two-fold and three-fold xylan in spruce. (c) The interior (yellow) and surface (cyan) glucan chains of cellulose have distinct hydroxymethyl conformation and NMR signals (from eucalyptus). The cross-section view of a hypothetical 18-chain model for an elementary cellulose fibril is shown. (d) Scheme of a large bundle formed by three elementary cellulose microfibrils. The high-order assembly forms the basis for many different structural environments for the glucose residues. (e) Acetylation and methyl-esterification change the ^{13}C chemical shifts of the carbonyl group (measured on *Arabidopsis*). The structures of three galacturonic acid residues, a component commonly found in pectin, are shown to match the NMR peaks. These panels are reconstituted from three previous publications [11,26,27].

monly found in hemicellulose and pectin. Arabinose can accommodate linkages at carbons 1, 2, 3, and 5. The 1,5-linked arabinose (also named 5-Ara) is featured with a uniquely large C5 chemical shift of 68–70 ppm, instead of the regular 62–63 ppm value for the terminal arabinose residues (t-Ara). Similarly, an additional linkage at carbon 2 will change the isotropic ^{13}C chemical shifts of C2 from 80–82 ppm to 88–90 ppm.

Second, from plant to plant, the composition of cell walls and even the composition of monosaccharide units within the same type of polysaccharide (e.g., xylan) can differ dramatically. For instance, the sidechain residue in the hemicellulose xylan is mainly arabinose (thus named arabinoxylan) in the softwood spruce, but changes to glucuronic acid (thus named glucuronoxylan) in the hardwood eucalyptus [11] (Fig. 2b). Fortunately, the signals of these sidechains can be differentiated (spectra available in ref. [11]).

Third, the next factor is the broad distribution of conformations in native polysaccharides. The hemicellulose xylan is typically found in two-fold (flat-ribbon) or three-fold (non-flat) helical screw conformations [11,28–30], which can be resolved using the signals of C4 and C1, the two important carbon sites for the glycosidic bond along the xylan backbone (Fig. 2b). Moreover, a continuous band of xylose C4 signals has also been observed in dried stems of *Arabidopsis* and the hydrated stems of hardwoods (eucalyptus and poplar) [11,29], as a result of the coexistence of many intermediate conformations between the two-fold and three-fold conformers. For cellulose, the surface and interior glucan chains have distinct hydroxymethyl conformations and resolvable signals (Fig. 2c). The dominant conformation is *gauche-trans* (*gt*) for surface chains and *trans-gauche* (*tg*) for interior chains, as recently determined using ^{1}H–^{1}H distance measurement [31].

Fourth, the high-order assembly of macromolecules also contributes to peak multiplicity. Since 2016, we have been consistently observing 7 major types of glucose units (namely types a-g) for the cellulose in the native cell walls of *Arabidopsis*, *Brachypodium*, maize, switchgrass, rice, spruce, eucalyptus, and poplar (see the representative spectrum in Fig. 2c). In the cross-section of a cellulose microfibril, the outer layer contains two types of surface chains (types f and g) with differentiable levels of water association, which has been examined using the water-edited ^{1}H polarization transfer method [31]. As a result, connections have been made between these two types of glucan chains with the concepts of hydrophobic and hydrophilic surfaces widely used in cellulose research, but further investigations are needed to assess this hypothesis. Types a and b are directly underneath the surface layer and exhibit strong cross peaks with surface chains [32,33]. The origin of type-c has remained vague for long. Type-c chains failed to show strong cross peaks with surface chains; therefore, it is supposed to be deeply embedded in the core so that it is separated from the surface chains by an intermediate layer (types a and b). However, the prevalent 18-chain model of a cellulose microfibril (as shown in Fig. 2c) could not accommodate such structural complexity. The presence of type-c chains can be better justified by the existence of larger bundles formed by multiple microfibrils as shown in Fig. 2d. The other two forms (d and e) have noticeably weaker signals. In addition, there are ongoing efforts using density functional theory calculations to connect structural variables, such as hydrogen bonds and other torsional angles, to the observed ^{13}C chemical shifts of cellulose [34,35].

Finally, chemical modifications, primarily acetylation and methyl esterification, are carried out by corresponding enzymes. The well-resolved carbonyl peaks (Fig. 2e) and methyl signals

can be used for distinguishing these functional groups and identifying their occurrence sites in cell wall polysaccharides [27,29,36,37]. The connection between the NMR fingerprint and the structural complexity is exemplified using plant carbohydrates but the five general principles are appliable to polysaccharides in other organisms.

4. Biochemical and ssNMR strategies to facilitate resonance assignment

Nowadays, resonance assignment is no longer a barrier for well-studied materials (e.g., bacteria and plants), but additional caution should be taken when dealing with uncharted biosystems. In this scenario, the best strategy is to combine ssNMR with chemical and genomics approaches. Chemical assays, such as compositional and linkage analyses, should be conducted to guide and validate the NMR assignment. When ambiguity arises, the ssNMR assignment can be validated by either generating mutant lines or using chemical extracts that selectively deplete the carbohydrate component of interest, thus rendering the corresponding signals absent in the spectra. An alternative is to compare with other species that are known to lack such molecules. When *Arabidopsis thaliana* was first studied using 2D and 3D ssNMR, a xyloglucan-deficient mutant and a pectin-depleted cell wall were compared with the wild-type plant [38,39]. A similar strategy was applied to the model fungus *Aspergillus fumigatus*, for which a collection of mutants depleting chitin, α-1,3-glucan, galactomannan, and galactosaminogalactan were generated [13].

A carbohydrate platform, complex carbohydrate magnetic resonance database (CCMRD), was created in 2019 to index the results from publications containing high-resolution ssNMR spectra and well-validated assignments [40]. Started from the 450 entries available in 2019 [40], the number of entries has increased to 720 as of Spring 2022. The database was designed to accommodate the prolific growth of datasets in upcoming years, in preparation for implementing automated approaches to encourage more ssNMR studies of carbohydrate systems [41,42].

Sequential assignment experiments (e.g., NCACX and NCOCX) have been extensively employed in protein ssNMR, but there are no equivalent methods for carbohydrates. This is partially due to the high degree of polymerization and the lack of nitrogen sites in most carbohydrates. However, novel carbohydrate sequencing strategies, analogous to those used in solution NMR [44], might be promising in solids for small polysaccharides with highly variable monosaccharide structures or with nitrogenated sugar units. This possibility needs to be explored.

3D ^{13}C correlation experiments provide additional spectral resolution over the 2D spectra and have been applied to biomass characterization [29,38]. Recently, a 3D ^{13}C DQ-SQ-SQ correlation experiment has been successfully employed to resolve the polysaccharide signals in the never-dried stems of spruce [43]. This experiment is free of the cube's body-diagonal, and the involvement of the DQ chemical shifts in the F1 dimension allows simultaneous observation of two parallel lines of signals in the F2-F3 planes for each coupled spin pair, e.g., s5-s6 and i5-i6 shown in Fig. 3a, b. The experiment is also useful for identifying long-range correlation cross peaks when a long-mixing ^{13}C–^{13}C mixing was implemented (Fig. 3c). Novel 3D experiments, such as those involving underexplored nuclei (e.g. ^{1}H and ^{17}O for carbohydrates) [45–47], should be developed to counterbalance the lack of nitrogen sites in regard to proteins.

5. Underutilized structural data for determining the packing interface

The ssNMR technique also provides information on the spatial proximities of biopolymers, which is its most appreciated capability, besides quantification, for investigating cell wall materials. A recent study of the plant secondary cell walls has proposed three comparative models for the secondary cell wall organization and the lignin-carbohydrate interface in the grass, hardwood, and softwood (Fig. 4) [11]. The function of hemicellulose xylan is found to be conformation-dependent: coating the even surface of cellulose via its flat-ribbon structure and primarily binding lignin domains via its non-flat conformation using preferential surface contacts stabilized by numerous electrostatic interactions. However, this selectivity is partially compromised in the stems of woody plants, with some of the lignin particles closely packed with the flat-ribbon part of xylan as well as the surface of cellulose fibrils, which is likely forced by molecular crowding in the densely packed stems of trees. Finally, the softwood spruce has the best molecular mixing of biopolymers on the nanoscale, with lignin adapting a dispersive distribution instead of forming nanoparticles.

Although over-simplified, these cartoon illustrations were built on the structural concepts derived from more than 1,172 site-specific ssNMR data [11,30]. The constantly improving resolution

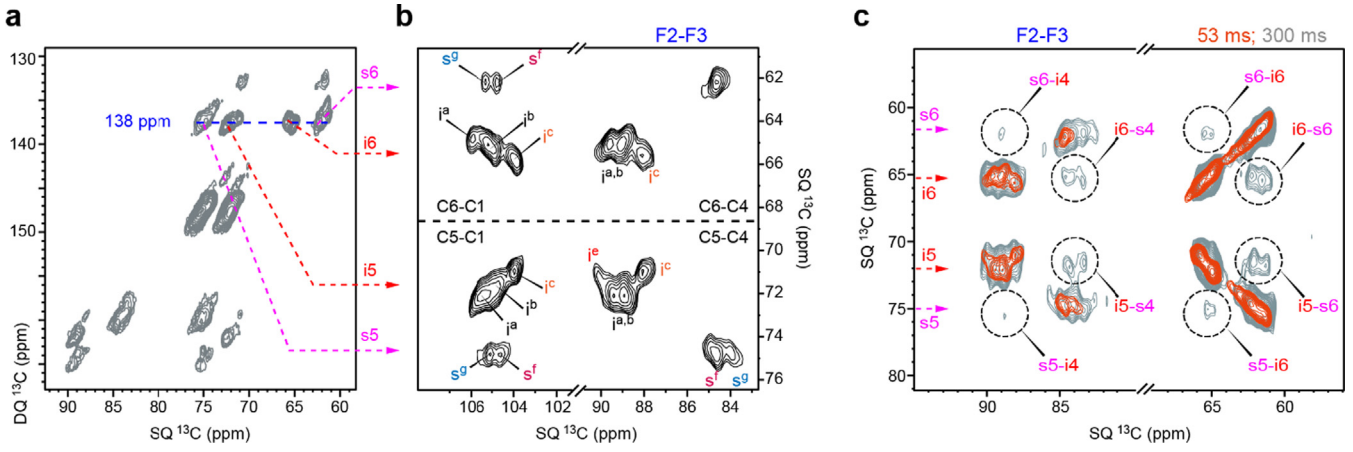

Fig. 3. 3D correlation experiments for resonance assignment and structural determination. (a) Representative F1-F3 plane of a 3D refocused-INADEQUATE-CORD spectrum of spruce (with CORD recoupling turned off). (b) 2D F2-F3 plane of spruce extracted from a 3D spectrum (with 53 ms CORD) at F1 = 138 ppm. (c) Long-range inter-chain interactions in spruce cellulose highlighted using dash line circles. The F2-F3 planes (F1 = 138 ppm) of 3D spectra measured with short (53 ms) and long (300 ms) CORD mixing periods were compared to uncover low-intensity but highly relevant cross peaks reporting intermolecular interactions. (Adapted from Shekar *et al.*) [43].

allows us to differentiate more carbon sites, and naturally a larger number of long-range cross peaks between these carbons. The complete dataset includes 508 intermolecular cross peaks (272 cross peaks in woody plants and 234 cross peaks in model plants), 475 ^{13}C-T_1 and ^{1}H-$T_{1\rho}$ relaxation time constants, and 189 water-edited intensities for various carbon sites. Nowadays, each pair of 2D ^{13}C–^{13}C correlation spectra (with long and short mixing times as contrast) allow the identification of 90–100 intermolecular cross peaks in a plant sample (Fig. 5a).

As shown in polymer contact maps (Fig. 5b), intermolecular cross peaks are categorized by their intensities following different chemical or structural motifs, such as the acetyl (Ac) and furanose ring of xylan (Xn) in two-fold or three-fold (2f/3f) screw conformations, the interior (i) and surface (s) chains in cellulose, as well as the ring carbons of guaiacyl (G) and syringyl (S) monolignol units, and the methoxyl (OMe) groups of lignin. In this way it is straightforward to recognize the structure selectivity of molecules in forming physical contacts: lignin primarily interacts with xylan instead of the other carbohydrate component (i.e., cellulose), and the S-residue contributes more to lignin-carbohydrate packing in poplar when compared with the G-residue. In particular, numerous strong cross peaks were identified in spruce, revealing the unique architecture of softwood and the homogeneous mixing of biopolymers happening on the nanoscale [11]. This systemic treatment of data allowed us to efficiently summarize the principal interactions stabilizing the polymer interface, but we still lack a method of converting the overwhelmingly abundant spectroscopic data into structurally meaningful physical models.

Unfortunately, the analyses of water-association and motional dynamics are even cruder. We rely on these data to distinguish the rigid and mobile domains of polymers, and to differentiate the hydrophilic matrix from the hydrophobic centers of the cell walls. Two polymers tightly packed to form larger aggregates are expected to show reduced mobility and water permeability, in addition to strong intermolecular cross peaks. These features were spotted for the chitin-α-glucan cores in the fungal cell wall of *Aspergillus fumigatus* [12,13] and the cellulose-two-fold-xylan core in plant secondary cell walls [11,30]. In contrast, molecules well dispersed in the matrix should be better solvated and more dynamic, expecting fewer and weaker cross peaks with other components. This trend has been observed in the β-glucan matrix of fungi and the hemicellulose-pectin matrix of plants. A complication arises as a single polysaccharide may have multiple domains with distinct dynamics. For instance, the pectin in *Arabidopsis* has

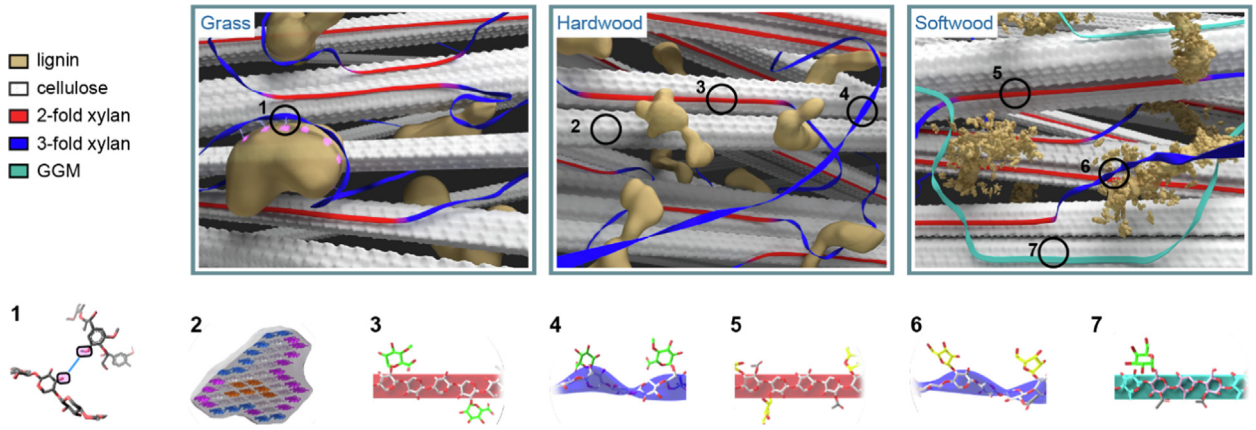

Fig. 4. Illustrative cartoons of biopolymer packing in different plant species restrained by ssNMR. The scheme summarizes the structural concepts summarized from 1,172 site-specific data regarding lignin (yellow), cellulose (white), xylan in two-fold (red, flat-ribbon) and three-fold (blue, twisted bands) screw conformations, and mannan (GGM, green). The structures of polymers are shown for seven regions. Figure adapted from reference [11].

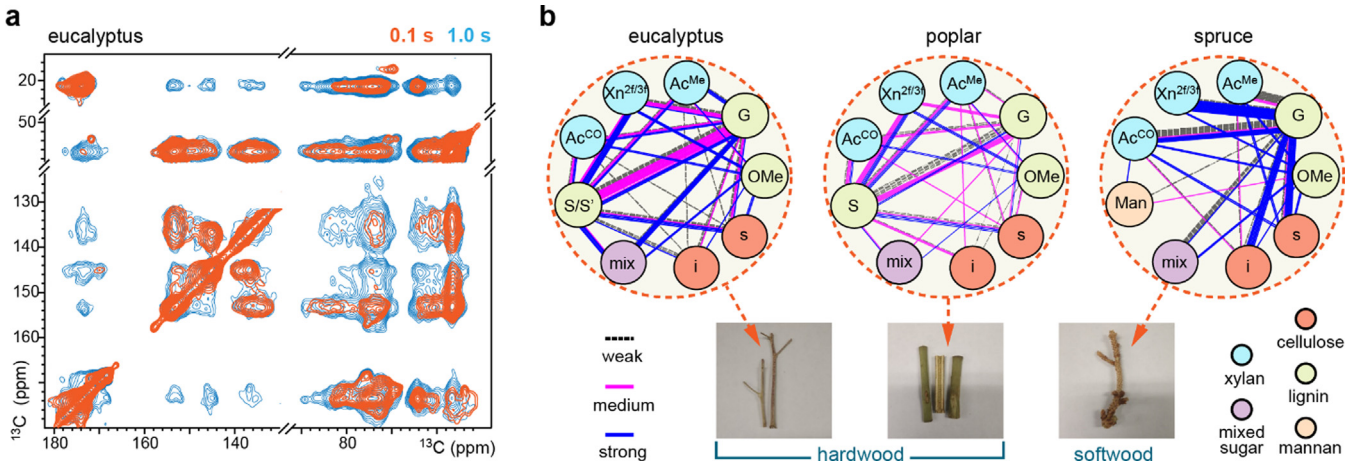

Fig. 5. Structural restraints on polymer packing. (a) Overlay of 2D dipolar-gated PDSD spectra with short (0.1 s; orange) and long (1.0 s; cyan) mixing times resolving 98 intermolecular cross peaks in eucalyptus. (b) Polymer contact map summarizing 272 intermolecular cross peaks arising among different structural units of xylan (cyan), lignin (lime/yellow), cellulose (red), mannan (light orange), and mixed sugars (purple). All cross peaks are categorized as strong (blue), medium (magenta), and weak (black dash lines) following their intensities. Pictures of the samples used for NMR characterization are shown. Figures adapted from reference [11].

a mobile domain forming the matrix that is prone to alkali extraction as well as an alkali-resistant and stiff domain that is packed with cellulose microfibrils [21].

Data analysis in this polymer/residue-specific manner has made it straightforward to cross-inspect different samples (e.g., from different species or mutant lines), but it has compromised the advantage of high-resolution site-specific data. We are facing the challenge of converting structural restraints into an energy-minimized ensemble of macromolecular structures. Inputs from experts in modeling and structural calculation will be highly valued.

6. Critical factors of MAS-DNP on cell wall samples

Nowadays, MAS-DNP is regularly used for characterizing cell walls by providing the needed sensitivity for visualizing the interface between lowly-populated polymers (compared to the bulk of the cell wall) and by enabling high-resolution characterization of unlabeled materials using 2D ^{13}C correlation experiments at natural isotopic abundance (1.1%) [48–52]. These applications have been reviewed recently [53]. Here we will mainly address two frequently asked questions regarding 1) how to ensure homogeneous hyperpolarization throughout the biomaterial being studied, and 2) how to mitigate the line-broadening effect due to the low temperature of the sample (e.g., ~100 K for MAS-DNP) and the paramagnetic effect from the radicals.

It is expected that samples with homogenous hyperpolarization should show comparable patterns in 1D ^{13}C spectra measured with and without microwave (MW) irradiation (Fig. 6a). Occasionally, lipid polymers and membranes may be poorly polarized. Lipid polymers mostly form separated domains and their signals are distinguishable from carbohydrate peaks, thus alleviating the interference. Cell walls are porous layers on the surface of the cell that can be freely accessed and easily penetrated by the biradicals dissolved in solution [54], which are small molecules only 2–3 nm across [55,56]. The polarization of electron spins will be first transferred to the ^{1}H in the biradical [57–59], and then to those in the solvent, and finally spread over a very long range via ^{1}H–^{1}H spin diffusion, which ensures homogeneous hyperpolarization, for example, across at least tens of nanometers as estimated using wood fibers [60]. This is the case for carbohydrates as the nuclear relaxation times are long enough at low temperature, unlike the lipids that still relax quickly.

Cellulose can largely retain its linewidth at the cryogenic temperature of DNP due to its high crystallinity (Fig. 6b, c) [50,61]. Indeed, we have observed impressively narrow full width at half maximum (FWHM) linewidths of 0.9–1.0 ppm for cotton cellulose on a 600 MHz/395 GHz MAS-DNP, which allowed us to track the glucose units in the Iα and Iβ model allomorphs frequently observed in model cellulosic materials [49]. The C-H dipolar order parameters are typically larger than 0.85 for cellulose; therefore, motion is not a major factor to consider for these fibrils. In contrast, hemicellulose and pectin are highly dynamic, and their signals are broadened out at a low temperature as shown in Fig. 6b. The resulting structure contains conformers with different isotropic chemical shifts, which inhomogeneously broaden the NMR lines. Despite this limitation, some peaks of these mobile components have been recently resolved in 2D ^{13}C–^{13}C correlation MAS-DNP spectra [50]. Under most circumstances, biradicals mainly stay in the solvent instead of being packed with biomolecules. Therefore, the paramagnetic relaxation enhancement effect from the biradicals is neither pronounced nor an issue for biomaterial DNP (Fig. 6c), especially for the solutions with a low concentration (5–10 mM) of radicals [62].

7. Expanding the application of MAS-DNP in carbohydrate research

For most cell wall molecules in rice stems, it has been shown that the linewidths in 2D ^{13}C correlation spectra collected on a 600 MHz/395 GHz MAS-DNP were comparable to those collected on a 400 MHz conventional ssNMR [50]. This is observed not only

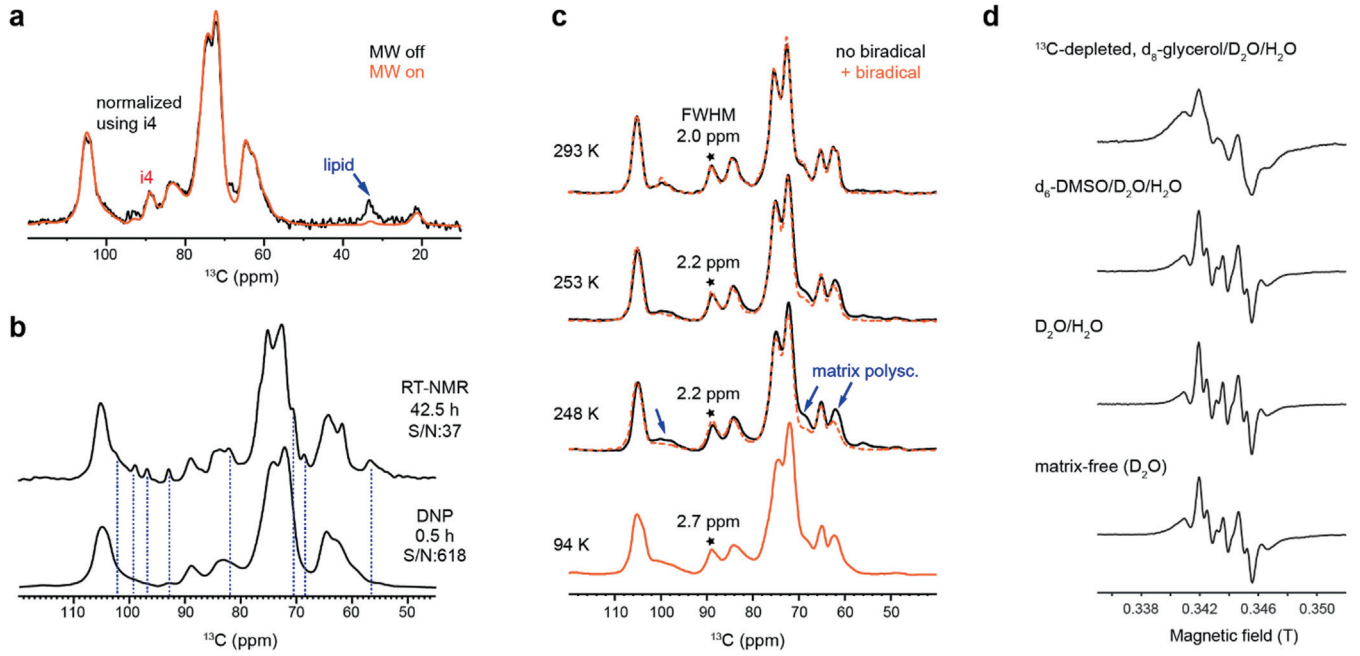

Fig. 6. Evaluation of sample and biradical conditions for MAS-DNP. (a) Uniform hyperpolarization across the cell wall confirmed by the consistent patterns of carbohydrate signals in the microwave-on (MW on) and microwave-off (MW off) spectra when normalized by the interior cellulose carbon 4 peaks (i4). Lipid components are not well polarized. (b) Time saving and improved signal-to-noise ratios of DNP over room-temperature NMR (RT-NMR). Blue dash lines indicate the signals of mobile components of rice stems broadened by the cryogenic temperature of DNP. (c) ^{13}C spectra of extracted *Arabidopsis* cell walls at different temperatures and biradical conditions. (d) Room temperature EPR spectra of AMUPol at 9.6 GHz in four rice stem samples (enhancement factor $\varepsilon_{on/off}$ of 38–57 on 600 MHz/395 GHz MAS-DNP) prepared using different solvents and procedures. The figures are remade from references [50,61].

for cellulose but also for some rigid portions of matrix polymers, such as the backbone of xylan. However, the most dynamic components, such as the arabinose sidechains of xylan, still evades DNP detection. The current resolution allowed for resonance assignment and compositional analysis of unlabeled cell wall materials. In the same study, the MAS-DNP analysis was further combined with room-temperature measurements (by conventional ssNMR) of relaxation and dipolar order parameters, providing a more complete assessment of these unlabeled samples [50]. However, an unaccomplished task is to develop methods that can efficiently detect intermolecular cross peaks under natural isotopic abundance [63].

Further questions include whether we can better handle matrix polysaccharides and other mobile components such as intracellular molecules. Finding answers to these questions might introduce new applications of MAS-DNP to biomaterial characterization. It is also unclear though if MAS-DNP at higher fields would help resolve the resolution issues. If the line-broadening is inhomogeneous, higher fields will not help, otherwise higher magnetic fields are desirable. However, in most cases, MAS-DNP at 800 MHz/527 GHz or higher generates lower enhancement in general. Ongoing progress notably in biradical design might improve MAS-DNP at high field [56,64,65]. It should be noted that smaller rotors (e.g., 1.3 mm) [66,67] are needed to improve the enhancement, but the use of a small rotor sacrifices the absolute sensitivity during ^{13}C detection as compared to the conventional 3.2 mm rotors. Overall, high-field DNP bears some promises but still presents major challenges and may not surpass the sensitivity provided by the lower-field DNP setups used today.

Unexpectedly, optimizing DNP samples, especially for the mixing protocol of biradical (in the solvent) and the cell wall material, is still fully empirical at this stage. Typically, the most limiting step of a MAS-DNP project is finding a sample preparation maximizing the sensitivity by both a great enhancement factor and a relatively short DNP buildup time. This often requires re-processing the samples with solvents and radicals for multiple cycles, by trial and error. Recently, a benchtop EPR was used to examine a collection of rice samples before subjection to MAS-DNP measurements (Fig. 6d). The EPR spectra suggest that the biradicals are favorably partitioning into the solvent in the samples with good sensitivity enhancement ($\varepsilon_{on/off}$ of 38–57). It will be beneficial if a protocol could be developed to rapidly screen the condition of radicals in the samples and pick up the most promising ones. This thematic is presently becoming even more relevant with the introduction of new radicals to the commercially available library.

The next question is how to place MAS-DNP into the context of other structural and biophysical techniques. Cryo-EM has established a leading role in protein structure determination and viral research but is not frequently used for carbohydrates or biomaterials. We have developed a strategy for analyzing the structures of unlabeled biomaterials by combining the nanoscale resolution of cryo-electron tomography (CET) with the atomic-level information provided by MAS-DNP (Fig. 7) [68]. CET of a cellulose fibril (cross-sectional FWHM width of 5.2–5.7 nm) revealed periodic structure along the fibril axis formed by two wrapped, yet not twisted filaments, each of which generally agrees with an 18-chain model for elementary cellulose microfibril. MAS-DNP resolved the carbon sites of interior and surface glucan chains, and intensity quantification supports the 18-chain arrangement with a relatively low extent of fibrillar bundling. The sample used was cellulose fibrils synthesized *in vitro* by protein machinery isolated from moss, which provided a simplified target for this successful attempt. It remains to be seen if DNP has synergism with cryo-EM for investigating more sophisticated polysaccharides and biopolymer complexes such as cell walls.

8. Conclusion

Over the last decade, significant advances have been made in the structural characterization of cell walls and carbohydrate-based biomaterials. However, due to the high heterogeneity of these cellular samples and the unique structural complexity of carbohydrates, the tools currently available for polymer research and protein structural biology are not fully applicable here. Development of semi-automatic tools for facilitating resonance assignment, novel pulse sequences and structural calculation methods for carbohydrate structural determination, as well as new radicals and optimized protocols for the application of high-field MAS-DNP may lead to breakthroughs in carbohydrate and biomaterial research.

9. Questions and Answers

(1) *The authors note that ssNMR resonance assignments for fungal and plant cells are complicated by a plethora of polysaccharide types, polymorphs of a given polysaccharide, covalent linkage patterns, and chemical modifications. Among the strategies used by the authors to resolve the resulting ambiguities are compositional and linkage analyses of smaller carbohydrate structures, but these options would seem to be precluded for recalcitrant materials such as lignified wood or melanized fungal cell walls. How serious is that limitation?*

Answer: Analyses of the carbohydrate components in woody materials have been reported in literature, for example, from MS and chromatography methods [69]. The analysis of lignin mainly relies on solution NMR methods [70]. These assays, though being destructive and requiring solubilization and chemical reactions before analysis, provide the knowledge needed for assigning the signals observed in solid-state NMR spectra. For melanized fungi, these biochemical assays involving the digestion and solubilization of the carbohydrate components should still be feasible [71]. For example, the structural concept of the conidium cell walls of *A. fumigatus*, which has melanin and rodlet layers outside the cell walls, have been summarized based on several decades of studies of carbohydrate linkage and composition [72].

(2) *In DNP-enhanced experiments, what are the best approaches to optimize hyperpolarization of composite materials that typically display a range of hydrophilic characters, cross polarization capabilities, or other physicochemical attributes? Are there good criteria for choosing particular biradical types without empirical optimization?*

Answer: It is difficult to derive universal principles as the biopolymers themselves and the composites they formed exist as highly heterogeneous and variable structures and carry diverse properties. However, a general expectation is that homogeneous distribution of biradicals to the porous biomaterial is key to achieving satisfactory hyperpolarization. Therefore, materials with a higher degree of polymer aggregation, higher hydrophobicity, and reduced porosity should be processed more thorough to better mix with the radicals. This has been sensed during the studies of secondary plant cell walls, which are significantly stiffer and denser than the primary cell walls. Still, systematic experimental validations are needed to establish correlations between preparation procedures, sample properties, as well as DNP enhancement and buildup times. The new families of radicals, such as the computationally designed AsymPolPOK and the TinyPol designed for high-field DNP, have shown significant improvement over AMUPol.

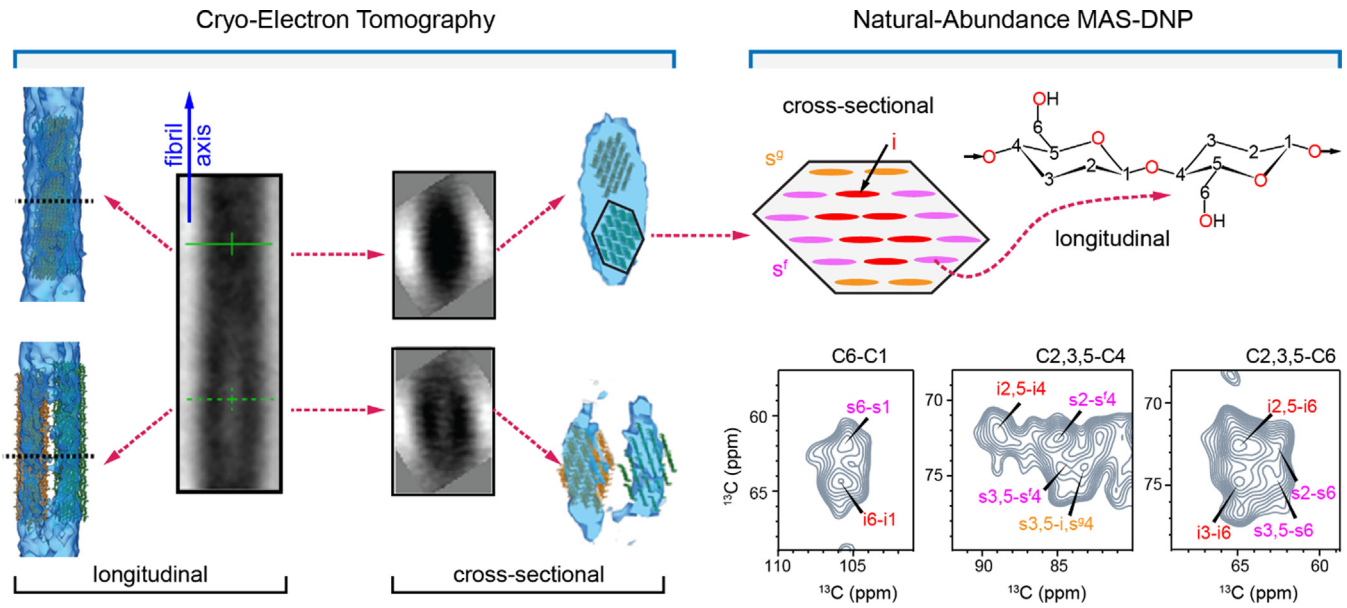

Fig. 7. Synergism of Cryo-EM and DNP for carbohydrate characterization. Subtomogram averages of *in vitro* fibers and isosurface rendering of the density map (left) reveal a fibril structure formed by two wrapped filaments. Each filament fibril can be fit to an 18-chain cellulose model, where the conformational distribution of glucan chains and the surface-to-interior ratio are analyzed by MAS-DNP (right). A 2D $^{13}C-^{13}C$ CHHC spectrum is included here to show the spectral resolution. Adapted from Deligey et al. [68].

(3) *The authors acknowledge the incompletely fulfilled promise of ssNMR-derived structural data to constrain detailed models of how the various biopolymers pack together to form a functionally versatile biomaterial in plants, animals, or fungi. The cartoons drawn from NMR-derived spatial proximities reveal, for instance, that lignin interacts primarily with xylan rather than cellulose and the syringyl residues of lignin monolignols contribute more than guaiacyl residues to intercomponent packing. What specific types of computational assistance would be useful for developing more definitive models of macromolecular structure based on constraints from ssNMR?*

Answer: There are several computational methods that could build physical models on different length scales that could help the interpretation and/or validation of ssNMR data. Atomistic molecular dynamics modeling with inputs from ssNMR constraints might be of the highest priority [73,74]. Ensemble averaged structures of lignocellulosic composites and the key thermodynamic parameters should deepen our understanding of the cell wall materials. DFT calculation might be used to assist the interpretation of observed NMR chemical shifts and visualize the local interface of polymer packing [35,76]. To further bridge the gaps between the NMR-derived structural concepts and the mechanical properties of bio-composites, coarse-grain modeling might be used [75]. The combination of ssNMR experimental data with assorted modeling and calculation approaches have the great potential of advancing the research of biomaterials.

(4) *What types of experiments were used to assign ^{13}C signals separately to surface and interior glucan chains, as shown in Fig. 2c? Please provide additional information about the details of the assignment approach for this specific case.*

Answer: The attributions of the surface and interior chains were determined by the spatial proximities of these glucan chains with matrix polymers (through proton-driven spin diffusion) and external water molecules (through water-edited ^{1}H polarization transfer). First, surface chains dominate the interactions of cellulose with matrix polymers. This was evidenced by their high equilibrium intensities analyzed using the build-up curves of cellulose-pectin cross-peak intensities as extracted from a series of 2D proton-driven spin diffusion spectra measured with varied mixing times up to 1.5 s [77]. Second, the surface chains have shown substantially faster ^{1}H polarization transfer from water molecules when compared to the internal chains [31].

(5) *In MAS NMR experiments near room temperature, do specific components of plant cell wall materials become visible under "solution NMR" measurement conditions (e.g., low-power decoupling, polarization transfers driven by scalar couplings)? Do other components have intermediate motional characteristics, for example as indicated by short $T_{1\rho}$ values or weak 13C–^{13}C cross peaks in 2D or 3D spectra with dipolar-coupling-based mixing periods? Which components?*

Answer: At ambient temperature and low MAS frequencies (e.g., 10–20 kHz), the most mobile and highly solvated molecules or polymer domains could be detected using "solution NMR" conditions. A notable example is arabinose, which can be efficiently detected using the refocused INEPT experiment that relies on scalar couplings for polarization transfer. Arabinose units form the branched sidechains of pectic polymers, being the most mobile component of the primary plant cell walls. Also, the backbones of pectic polymers (homogalacturonan and rhamnogalacturonan) have also been observed in refocused INEPT spectra, but with considerably lower intensities as they are only intermediately mobile. As a result, homogalacturonan and rhamnogalacturonan also suffer significantly from long dipolar-coupling-based mixing periods. To compensate for this effect, moderately low temperature is thus required to partially immobilize these two polymers in order to observe their intermolecular cross peaks with other cell wall components such as cellulose.

When extending to moderately fast MAS (e.g. 50 kHz), the dynamic nature of pectic polymers permit the detection of their ^{1}H signals with narrow linewidths, without the requirement of deuteration or ultrafast MAS (e.g., above 100 kHz). This strategy has been demonstrated recently by Phyo and Hong [45], presenting a promising direction for plant solid-state NMR.

(6) *Approximately how many research labs are currently using NMR to characterize plant cell wall materials? In which countries are they located? Are they supported exclusively by government agencies, or are some of these labs supported by industry or located within commercial entities?*

Answer: We have been keeping close track of the studies from 45 research labs using NMR to characterize plant cell wall materials, which have inspired our research program and have been frequently cited in our recent publications. These labs are distributed worldwide, including USA, France, UK, Sweden, Finland, Spain, Italy, Japan, China, India, Australia, New Zealand, Brazil, etc. A list of the principal investigators is provided in the response letter to the reviewers' comments but will not be included here due to the limited space. Most of these groups are in universities and national laboratories, but we are also aware of several labs in the industry of wood, pulp, and bioenergy. Due to our limited knowledge, we believe there are many more research groups, especially for the field of solution NMR research. Indeed, we recently indexed the annual number of plant NMR publications between 1991 and 2020 registered on Web of Science. There are around 1200 publications, 90% of which were studies conducted using solution NMR methods.

Declaration of Competing Interest

The authors declare that they have no known competing financial interests or personal relationships that could have appeared to influence the work reported in this paper.

Acknowledgments

This work was supported by the U.S. Department of Energy (grant no. DE-SC0021210). F.D. was supported as part of the Center for Lignocellulose Structure and Formation, an Energy Frontier Research Center funded by the US Department of Energy, Office of Science, Basic Energy Sciences under award number DE-SC0001090. The National High Magnetic Field Laboratory is supported by National Science Foundation through NSF/DMR-1644779 and the State of Florida.

References

[1] J. Duus, C.H. Gotfredsen, K. Bock, Carbohydrate Structural Determination by NMR Spectroscopy: Modern Methods and Limitations, Chem. Rev. 100 (2000) 4589–4614.
[2] R.H. Atalla, D.L. Vanderhart, Native cellulose: a composite of two distinct crystalline forms, Science 223 (1984) 283–285.
[3] M. El hariri El Nokab, et al., Solid State NMR a Powerful Technique for Investigating Sustainable/Renewable Cellulose-Based Materials, Polymers 14 (2022) 1049.
[4] M. Foston, Advances in solid-state NMR of cellulose, Curr. Opin. Biotechnol. 27 (2014) 176–184.
[5] N. Ghassemi et al., Solid-State NMR Investigations of Extracellular Matrices and Cell Walls of Algae, Bacteria, Fungi, and Plants, Chem. Rev. 122 (2021) 10036–10086.
[6] C. Reichhardt, L. Cegelski, Solid-state NMR for bacterial biofilms, Mol. Phys. 112 (2014) 887–894.
[7] J.E. Kelly, C. Chrissian, R.E. Stark, Tailoring NMR experiments for structural characterization of amorphous biological solids: A practical guide, Solid State Nucl. Magn. Reson. 109 (2020) 101686.
[8] A.A. Arnold et al., Whole cell solid-state NMR study of *Chlamydomonas reinhardtii* microalgae, J. Biomol. NMR 70 (2018) 123–131.
[9] B. Reif, S.E. Ashbrook, L. Emsley, M. Hong, Solid-state NMR spectroscopy, Nat. Rev. Methods Primers 1 (2021) 2.
[10] P.R.L. Markwick, T. Malliavin, M. Nilges, Structural Biology by NMR: Structure, Dynamics, and Interactions, PLoS Comput. Biol. 4 (2008) e1000168.
[11] A. Kirui et al., Carbohydrate-aromatic interface and molecular architecture of lignocellulose, Nat. Commun. 13 (2022) 538.
[12] X. Kang et al., Molecular architecture of fungal cell walls revealed by solid-state NMR, Nat. Commun. 9 (2018) 2747.
[13] A. Chakraborty et al., A molecular vision of fungal cell wall organization by functional genomics and solid-state NMR, Nat. Commun. 12 (2021) 6346.
[14] G. Hou, S. Yan, J. Trébosc, J.-P. Amoureux, T. Polenova, Broadband homonuclear correlation spectroscopy driven by combined R2nv sequences under fast magic angle spinning for NMR structural analysis of organic and biological solids, J. Magn. Reson. 232 (2013) 18–30.
[15] G.D. Paëpe, J.R. Lewandowski, A. Loquet, A. Böckmann, R.G. Griffin, Proton assisted recoupling and protein structure determination, J. Chem. Phys. 129 (2008) 245101.
[16] A. Lange, S. Luca, M. Baldus, Structural Constraints from Proton-Mediated Rare-Spin Correlation Spectroscopy in Rotating Solids, J. Am. Chem. Soc. 124 (2002) 9704–9705.
[17] C. Ader et al., Structural Rearrangements of Membrane Proteins Probed by Water-Edited Solid-State NMR Spectroscopy, J. Am. Chem. Soc. 131 (2009) 170–176.
[18] P.B. White, T. Wang, Y.B. Park, D.J. Cosgrove, M. Hong, Water-Polysaccharide Interactions in the Primary Cell Wall of Arabidopsis thaliana from Polarization Transfer Solid-State NMR, J. Am. Chem. Soc. 136 (2014) 10399–10409.
[19] J.K. Williams, K. Schmidt-Rohr, M. Hong, Aromatic spectral editing techniques for magic-angle-spinning solid-state NMR spectroscopy of uniformly ^{13}C-labeled proteins, Solid State Nucl. Magn. Reson. 72 (2015) 118–126.
[20] Y. Gao, J.C. Mortimer, Unlocking the architecture of native plant cell walls via solid-state nuclear magnetic resonance, Methods Cell Biol. 160 (2020) 121–143.
[21] T. Wang, Y.B. Park, D.J. Cosgrove, M. Hong, Cellulose-pectin spatial contacts are inherent to never-dried *Arabidopsis* primary cell walls: evidence from solid-state nuclear magnetic resonance, Plant Physiol. 168 (2015) 871–884.
[22] A. Poulhazan et al., Identification and Quantification of Glycans in Whole Cells: Architecture of Microalgal Polysaccharides Described by Solid-State Nuclear Magnetic Resonance, J. Am. Chem. Soc. 46 (2021) 19374–19388.
[23] Y. Gao, A.S. Lipton, Y. Wittmer, D.T. Murray, J.C. Mortimer, A grass-specific cellulose–xylan interaction dominates in sorghum secondary cell walls, Nat. Commun. 11 (2020) 6081.
[24] R. Cresswell et al., Importance of water in maintaining softwood secondary cell wall nanostructure, Biomacromolecules 8 (2021) 4669–4680.
[25] W. Zhao, L.D. Fernando, A. Kirui, F. Deligey, T. Wang, Solid-state NMR of plant and fungal cell walls: a critical review, Solid State Nucl. Magn. Reson. 107 (2020) 101660.
[26] T. Wang, A. Salazar, O.A. Zabotina, M. Hong, Structure and Dynamics of Brachypodium Primary Cell Wall Polysaccharides from Two-Dimensional 13C Solid-State Nuclear Magnetic Resonance Spectroscopy, Biochemistry 53 (2014) 2840–2854.
[27] A. Kirui et al., A pectin Methyltransferase modulates polysaccharide dynamics and interactions in *Arabidopsis* primary cell walls: Evidence from solid-state NMR, Carbohydr. Polym. 270 (2021) 118370.
[28] T.J. Simmons et al., Folding of xylan onto cellulose fibrils in plant cell walls revealed by solid-state NMR, Nat. Commun. 7 (2016) 13902.
[29] R. Dupree et al., Probing the Molecular Architecture of Arabidopsis thaliana Secondary Cell Walls Using Two- and Three-Dimensional 13C Solid State Nuclear Magnetic Resonance Spectroscopy, Biochemistry 54 (2015) 2335–2345.
[30] X. Kang et al., Lignin-polysaccharide interactions in plant secondary cell walls revealed by solid-state NMR, Nat. Commun. 10 (2019) 1–9.
[31] P. Phyo, T. Wang, Y. Yang, H. O'Neill, M. Hong, Direct determination of hydroxymethyl conformations of plant cell wall cellulose using ^{1}H polarization transfer solid-state NMR, Biomacromolecules 19 (2018) 1485–1497.
[32] T. Wang, H. Yang, J.D. Kubicki, M. Hong, Cellulose structural polymorphism in plant primary cell walls investigated by high-field 2D solid-state NMR spectroscopy and density functional theory calculations, Biomacromolecules 17 (2016) 2210–2222.
[33] T. Wang, M. Hong, Solid-state NMR investigations of cellulose structure and interactions with matrix polysaccharides in plant primary cell walls, J. Exp. Bot. 67 (2016) 503–514.
[34] H. Yang, J.D. Kubicki, A density functional theory study on the shape of the primary cellulose microfibril in plants: effects of C6 exocyclic group conformation and H-bonding, Cellulose 27 (2020) 2389–2402.
[35] H. Yang et al., Structural factors affecting 13C NMR chemical shifts of cellulose: a computational study, Cellulose 25 (2018) 23–36.
[36] T. Wang, Y. Chen, A. Tabuchi, D.J. Cosgrove, M. Hong, The target of β-expansin EXPB1 in maize cell walls from binding and solid-state NMR studies, Plant Physiol. 172 (2016) 2107–2119.
[37] O.M. Terrett et al., Molecular architecture of softwood revealed by solid-state NMR, Nat. Commun. 10 (2019) 4978.
[38] M. Dick-Pérez et al., Structure and interactions of plant cell-wall polysaccharides by two-and three-dimensional magic-angle-spinning solid-state NMR, Biochemistry 50 (2011) 989–1000.
[39] M. Dick-Perez, T. Wang, A. Salazar, O.A. Zabotina, M. Hong, Multidimensional solid-state NMR studies of the structure and dynamics of pectic polysaccharides in uniformly ^{13}C-labeled Arabidopsis primary cell walls, Magn. Reson. Chem. 50 (2012) 539–550.
[40] X. Kang et al., CCMRD: a solid-state NMR database for complex carbohydrates, J. Biomol. NMR 74 (2020) 239–245.
[41] D.-W. Li, A.L. Hansen, C. Yuan, L. Bruschweiler-Li, R. Bruschweiler, DEEP picker is a deep neural network for accurate deconvolution of complex two-dimensional NMR spectra, Nat. Commun. 12 (2021) 5229.

[42] M. Cordova, M. Balodis, B. Simoes de Almeida, M. Ceriotti, L. Emsley, Bayesian probabilistic assignment of chemical shifts in organic solids, Sci. Adv. 7 (2021) eabk2341.
[43] S.C. Shekar, W. Zhao, L.D. Fernando, I. Hung, T. Wang, A ^{13}C three-dimensional DQ-SQ-SQ correlation experiment for high-resolution analysis of complex carbohydrates using solid-state NMR, J. Magn. Reson. 336 (2022) 107148.
[44] C.J. Gray et al., Advancing Solutions to the Carbohydrate Sequencing Challenge, J. Am. Chem. Soc. 141 (2019) 14463–14479.
[45] P. Phyo, M. Hong, Fast MAS ^{1}H–^{13}C correlation NMR for structural investigations of plant cell walls, J. Biomol. NMR 73 (2019) 661–674.
[46] C. Bougault, I. Ayala, W. Vollmer, J.P. Simorre, P. Schanda, Studying intact bacterial peptidoglycan by proton-detected NMR spectroscopy at 100 kHz MAS frequency, J. Struct. Biol. 206 (2019) 66–72.
[47] J. Shen et al., Solid-state 17O NMR study of α-d-glucose: exploring new frontiers in isotopic labeling, sensitivity enhancement, and NMR crystallography, Chem. Sci. 13 (2022) 2591–2603.
[48] H. Takahashi et al., Rapid Natural-Abundance 2D ^{13}C–^{13}C Correlation Spectroscopy Using Dynamic Nuclear Polarization Enhanced Solid-State NMR and Matrix-Free Sample Preparation, Angew. Chem. Int. Ed. 51 (2012) 11766–11769.
[49] A. Kirui et al., Atomic resolution of cotton cellulose structure enabled by dynamic nuclear polarization solid-state NMR, Cellulose 26 (2019) 329–339.
[50] W. Zhao et al., Solid-state NMR of unlabeled plant cell walls: high-resolution structural analysis without isotopic enrichment, Biotechnol. Biofuels 14 (2021) 14.
[51] P. Berruyer et al., Advanced characterization of regioselectively substituted methylcellulose model compounds by DNP enhanced solid-state NMR spectroscopy, Carbohydr. Polym. 262 (2021) 117944.
[52] F.A. Perras et al., Atomic-level structure characterization of biomass pre-and post-lignin treatment by dynamic nuclear polarization-enhanced solid-state NMR, J. Phys. Chem. A 121 (2017) 623–630.
[53] A. Chakraborty et al., Biomolecular complex viewed by dynamic nuclear polarization solid-state NMR spectroscopy, Biochem. Soc. Trans. 48 (2020) 1089–1099.
[54] H. Takahashi et al., Solid-state NMR on bacterial cells: selective cell wall signal enhancement and resolution improvement using dynamic nuclear polarization, J. Am. Chem. Soc. 135 (2013) 5105–5110.
[55] C. Sauvée et al., Highly Efficient, Water-Soluble Polarizing Agents for Dynamic Nuclear Polarization at High Frequency, Angew. Chem. Int. Ed. 52 (2013) 10858–10861.
[56] F. Mentink-Vigier et al., Computationally Assisted Design of Polarizing Agents for Dynamic Nuclear Polarization Enhanced NMR: The AsymPol Family, J. Am. Chem. Soc. 140 (2018) 11013–11019.
[57] F. Mentink-Vigier, T. Dubroca, J. Van Tol, S.T. Sigurdsson, The distance between g-tensors of nitroxide biradicals governs MAS-DNP performance: The case of the bTurea family, J. Magn. Reson. 329 (2021) 107026.
[58] F. Mentink-Vigier, S. Vega, G. De Paëpe, Fast and accurate MAS–DNP simulations of large spin ensembles, Phys. Chem. Chem. Phys. 19 (2017) 3506–3522.
[59] F.A. Perras, M. Pruski, Large-scale ab initio simulations of MAS DNP enhancements using a Monte Carlo optimization strategy, J. Chem. Phys. 149 (2018) 154202.
[60] J. Viger-Gravel et al., Topology of pretreated wood fibers using dynamic nuclear polarization, J. Phys. Chem. C 123 (2019) 30407–30415.
[61] T. Wang et al., Sensitivity-enhanced solid-state NMR detection of expansin's target in plant cell walls, Proc. Natl. Acad. Soc. USA 110 (2013) 16444–16449.
[62] H. Takahashi, S. Hediger, G. De Paëpe, Matrix-free dynamic nuclear polarization enables solid-state NMR ^{13}C–^{13}C correlation spectroscopy of proteins at natural isotopic abundance, Chem. Commun. 49 (2013) 9479–9481.
[63] K. Märker et al., Welcoming natural isotopic abundance in solid-state NMR: probing π-stacking and supramolecular structure of organic nanoassemblies using DNP, Chem. Sci. 8 (2017) 974–987.
[64] W. Zhai et al., Postmodification via Thiol-Click Chemistry Yields Hydrophilic Trityl-Nitroxide Biradicals for Biomolecular High-Field Dynamic Nuclear Polarization, J. Phys. Chem. B 124 (2020) 9047–9060.
[65] A. Lund et al., TinyPols: a family of water-soluble binitroxides tailored for dynamic nuclear polarization enhanced NMR spectroscopy at 18.8 and 21.1 T, Chem. Sci. 11 (2020) 2810–2818.
[66] S.R. Chaudhari et al., Dynamic nuclear polarization at 40 kHz magic angle spinning, Phys. Chem. Chem. Phys. 18 (2016) 10616–10622.
[67] D. Wisser et al., BDPA-Nitroxide Biradicals Tailored for Efficient Dynamic Nuclear Polarization Enhanced Solid-State NMR at Magnetic Fields up to 21.1 T, J. Am. Chem. Soc. 140 (2018) 13340–13349.
[68] F. Deligey et al., Structure of In Vitro-Synthesized Cellulose Fibrils Viewed by Cryo-Electron Tomography and 13C Natural-Abundance Dynamic Nuclear Polarization Solid-State NMR, Biomacromolecules 23 (2022) 2290–2301.
[69] R.C. Pettersen, V.H. Schwandt, M.J. Effland, An Analysis of the Wood Sugar Assay Using HPLC: A Comparison with Paper Chromatography, J. Chromatogr. Sci. 22 (1984) 478–484.
[70] S.D. Mansfield, H. Kim, F. Lu, J. Ralph, Whole plant cell wall characterization using solution-state 2D NMR, Nat. Protoc. 7 (2012) 1579–1589.
[71] N.A.R. Gow, J.P. Latge, C.A. Munro, The Fungal Cell Wall: Structure, Biosynthesis, and Function, Microbiol Spectr 5 (2017).
[72] J.-P. Latgé, G. Chamilos, Aspergillus fumigatus and Aspergillosis in 2019, Clin. Microbiol. Rev. 33 (2019) e00140–00118.
[73] L. Petridis, J.C. Smith, Molecular-level driving forces in lignocellulosic biomass deconstruction for bioenergy, Nat. Rev. Chem. 2 (2018) 382–389.
[74] J.R. Perilla et al., Molecular dynamics simulations of large macromolecular complexes, Curr. Opin. Struct. Biol. 37 (2015) 64–74.
[75] Y. Zhang et al., Molecular insights into the complex mechanics of plant epidermal cell walls, Science 372 (2021) 706–711.
[76] H. Yang et al., Quantum calculations on plant cell wall component interactions, Interdis. Sci. 11 (2019) 485–495.
[77] T. Wang, O. Zabotina, M. Hong, Pectin–cellulose interactions in the *Arabidopsis* primary cell wall from two-dimensional magic-angle-spinning solid-state nuclear magnetic resonance, Biochemistry 51 (2012) 9846–9856.